Fracture Mechanics of Plate Debonding

P. M. M. Achintha[1] and C. J. Burgoyne[2]

Abstract: This paper presents a fracture mechanics model to determine the load at which FRP plates will debond from reinforced concrete beams. This will obviate the need for finite-element analyses to be used in situations where there is an infinite stress concentration and where the exact details of the interface geometry and properties are unknowable. The paper shows how fracture mechanics concepts based on energy release rates, can be used to answer the question "Will this existing interface crack extend?" Possible modes of debonding are analyzed as is the effect of the plate curtailment location on the debonding mode.

DOI: 10.1061/(ASCE)1090-0268(2008)12:4(396)

CE Database subject headings: Bonding strength; Cracking; Fiber reinforced polymers; Strain energy.

Introduction

The enhanced structural performance of reinforced concrete (RC) beams that have been strengthened by externally bonded fiber reinforced polymer (FRP) plates is strongly reliant on the effectiveness of the concrete-FRP interface. Strengthened beams often fail by premature plate debonding (Leung 2001); an understanding of the plate debonding mechanism is of the greatest important for the successful application of external FRP plates on RC beams. It is important to know where and when debonding initiates and the influence of parameters such as the plate curtailment location and the plate thickness. Over the last decade, much research has focused on the plate debonding failures, but the problems have not been fully resolved.

Two modes of plate debonding are experienced in simply-supported externally strengthened RC beams (Leung 2001) (Fig. 1); one initiates at a crack in the beam midspan zone and propagates towards the nearest beam end, while the other initiates at a plate end and propagates inwards. The first mode is termed *intermediate-crack induced debonding* or *midspan debonding* and the second mode is *plate-end debonding*. High interfacial stresses are present in the vicinity of an existing crack and at the plate end, which initiate these two debonding modes. The temptation is, therefore, to compute these interfacial stresses and compare them with interface strength properties to determine the failure loads.

However, the debonding mechanisms of plates glued to concrete structures are proving very difficult to analyze. The interface can be modeled using finite-elements, but this procedure is doomed to failure; a reentrant corner leads to an infinite stress concentration, so the values returned by a finite-element program are governed by the smallness of the elements used, and by unwarranted assumptions about adhesive properties that the analyst is forced to make.

Models based on linear-elastic theory have also been employed to determine the interface stresses at critical locations (i.e., at the plate ends and in the vicinities of existing flexural/flexural-shear cracks), which can then be compared with the interface shear strength obtained from small-scale shear lap tests (Pham and Al-Mahaidi 2006). However, the inevitable cracking and other nonlinearities inherent in RC elements violate the assumptions made in the derivation of the models, and it is also believed that shear lap tests do not simulate the actual debonding mechanism of real beams. In addition, the models generally predict unrealistic stress singularities at the plate ends.

Empirical formulations, mainly as design guides to eliminate plate debonding failures, can be found in the literature. ACI Committee 440 (ACI 440.2R-02) (ACI 2002) suggests limits on the FRP plate strain to prevent debonding, based on a database of test results, but the theoretical justification is unclear: These strain limits depend only on the stiffness properties of the FRP plates and do not take account of the concrete-FRP interface properties, width of the FRP plate, or the plate curtailment location, all of which would be expected to affect debonding.

Fracture-mechanics models, such as the Hutchinson and Suo interface fracture model for layered elastic materials (Hutchinson and Suo 1992) offer a better alternative for interface debonding problems. They assume that, since flaws are inevitable in the interface, what matters is whether these flaws can propagate. When an existing flaw extends, the energy needed to form associated new surfaces depends on the interface fracture energy and must be compared with the energy released by the system, which in turn depends on the change of stored strain energy. This idea has been applied in many fields: For example, to the analysis of interface fracture between dissimilar materials in electronic pack-

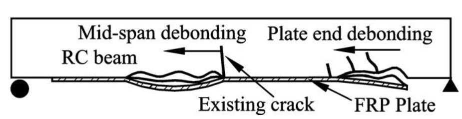

Fig. 1. Two modes of debonding

[1]Ph.D. Candidate, Dept. of Engineering, Univ. of Cambridge, Trumpington St., Cambridge, CB2 1PZ, U.K. E-mail: pmma2@eng.cam.ac.uk

[2]Reader in Concrete Structures, Dept. of Engineering, Univ. of Cambridge, Trumpington St., Cambridge, CB2 1PZ, U.K. (corresponding author). E-mail: cjb@eng.cam.ac.uk

Note. Discussion open until January 1, 2009. Separate discussions must be submitted for individual papers. To extend the closing date by one month, a written request must be filed with the ASCE Managing Editor. The manuscript for this paper was submitted for review and possible publication on December 20, 2006; approved on August 27, 2007. This paper is part of the ***Journal of Composites for Construction***, Vol. 12, No. 4, August 1, 2008. ©ASCE, ISSN 1090-0268/2008/4-396–404/$25.00.

ages (Kay et al. 2006); delamination failure between the thermal barrier coatings and load bearing alloy due to thermal expansion mismatch (Chen 2006); crack propagation along polymer-glass and polymer-metal interfaces (Vellinga et al. 2006); fatigue delamination in ductile interfaces in layered materials (Daily and Klingbeil 2006), and interface failures of patterned films undergoing a typical thermal excursion during the integration process (Liu et al. 2007). There is, however, only limited application to the study of concrete-FRP debonding failures (Hearing 2000; Günes 2004). Those studies only considered the energy change at the interface itself, whereas this work will show that consequential energy changes elsewhere in the beam are significant.

Hutchinson and Suo (1992) also studied the crack tip stress intensity factors, but they were considering materials for which linear-elastic fracture mechanics was appropriate. That approach is much more difficult in concrete because the materials are nonlinear and nonhomogeneous, so the path that the crack follows, and the detailed stress conditions, depend on the location of aggregate particles and other factors, which are unknowable. The fact that they obtained good agreement with their energy-based studies indicates that the approach adopted here should be a suitable method for the study of FRP debonding.

When an existing debonding crack extends, the determination of the associated *energy release rate* of the system is not trivial. A detailed analysis would require knowledge of the exact location of the reinforcement and each of the existing flexural/flexural-shear cracks, while the interface fracture energy depends on the interface microstructure, all of which are effectively unknowable. Thus, the objective is to develop methods to find both the energy release rate and the interface fracture energy to accuracies sufficient for practical purposes.

An essential first stage of this process is the determination of the strain energy in a beam, which in turn requires knowledge of the moment-curvature ($M-\kappa$) relations. That work, which is based on an extension of Branson's model (Branson 1968) to allow for tension stiffening, takes account of the axial force induced by the FRP plate (whether bonded or debonded), and the possible yielding of the original untensioned reinforcement in the beam. The model has been validated against test results in the literature. It has then been extended to determine the curvature after the beam has been unloaded, from which the strain energy of the beam can be determined. That work is described in a separate publication, which has been submitted for publication elsewhere (Achintha and Burgoyne 2006). This paper builds on that work to show how these fracture mechanics concepts can be used to answer the question "Will this existing interface crack extend?"

Fracture Mechanics for Plate Debonding

Since flaws are inevitable in the interface, what matters is whether an existing flaw can propagate. The proposed model first assumes a debonding crack of known length and orientation. The energy states of the beam are computed, both in this state and when the crack is further extended by a small distance δx. The energy released from the system due to the crack extension can then be determined from energy conservation concepts; part of this released energy is consumed to create the new fracture surfaces required for crack extension. The extension of the crack will occur only if there is sufficient released energy to create the required new surfaces. Thus, whether an existing debonding crack *will* propagate or not can be decided by comparing the possible available energy with the energy that is actually required. The energy needed to form associated new fracture surfaces depends on the interface fracture energy, the determination of which will be discussed later. The present discussion concentrates on the determination of the energy released from the system when an existing debonding crack extends.

Energy Released from the System When a Crack Extends

The force in the FRP plate (F_p) is chosen in such a way that the relevant compatibility condition between the FRP plate and the RC beam is satisfied (Achintha and Burgoyne 2006). If the FRP plate is perfectly bonded to the beam, then *strain* compatibility must be satisfied locally between the FRP plate and the strain in the tension fiber of the concrete. When the FRP plate has debonded, then the weaker condition has to be satisfied in which the *extension* of the plate in the debonded region is the same as the extension of the tension fiber in the concrete.

When the debonding crack extends, F_p in the debonded zone may alter to retain compatibility. This change in F_P causes alterations in the strain and stress profiles of the relevant RC sections, and, hence, the energy states alter, releasing some energy; the energy stored in the FRP plate itself also changes. At each boundary, where the debonded and the fully bonded zones are separated, a discontinuity in the value of F_p can be expected since its magnitude depends on different compatibility conditions on either side of the boundary. Sharp discontinuities in F_p cannot occur, so there must be a transition zone where there is relative slip between the FRP and the beam. The transition zone F_p profile depends on the difference between the two F_p values in the debonded and fully bonded areas. In the fully bonded region, F_p does not change unless the applied load changes (and in the present study, only the debonding crack initiation increment at constant load is considered), since the more rigorous strain compatibility condition still applies; it is the change in F_p in the *debonded zone* that causes variation in the F_p profile over the transition zone with a consequent energy release.

Sections in both the debonded and the transition zones release energy when the crack extends, which must be summed to obtain the total energy release at the crack tip. For a given section, it is important to know the amount of energy that is available for release.

When a RC beam bends, energy is put into the beam by the loads, some of which is dissipated in the concrete, either in flexural-tension cracking or material nonlinearity, and by yielding of the steel reinforcement, while the rest is recoverable and stored as strain energy. Thus, for a given section, only the stored strain energy that can be recovered when the beam is completely unloaded is active and will be responsible for the change of the energy state of the section upon debonding. The bending moment from which the unloading takes place, and the corresponding unloading $M-\kappa$ relations, are both required for the determination of the strain energy.

Strain Energy in a Strengthened Section

The $M-\kappa$ behavior of a strengthened section considers the FRP plate as an external prestressing element inducing both force and moment on the RC portion of the section (Fig. 2). It is convenient to consider separately the stress state in the original reinforced concrete beam, with its internal reinforcement, and the stress in the FRP plate. They will be related by a compatibility condition

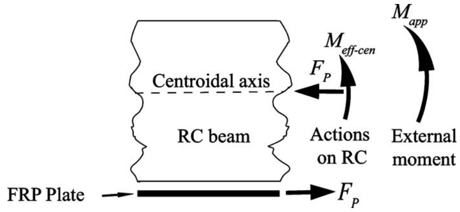

Fig. 2. Actions on a RC section

that alters when debonding occurs. The total strain energy (SE) in a strengthened section consists of three components: The SE in the RC beam due to flexure (flexural SE), the SE in the RC beam due to axial force (axial SE), and the SE in the FRP plate (FRP SE).

Flexural Strain Energy

It is assumed that all the constituents are linear elastic upon unloading, so the unloading $M-\kappa$ relations are linear irrespective of the moment from which the unloading takes place, although there will usually be some residual curvature if the load is completely removed. Thus, the flexural strain energy available in a beam segment of unit length depends on the moment applied to the RC element alone (the effective moment $M_{\text{eff-cen}}$) as shown in Fig. 3 and calculated from

$$\text{SE}_E\big|_{\text{flexure}} = \frac{1}{2}M_{\text{eff-cen}}\kappa_{\text{UL}} \tag{1}$$

where $M_{\text{eff-cen}}$ and κ_{UL}=effective moment on the RC section about the centroid of the RC beam itself, and the corresponding change in curvature upon complete unloading.

Axial Strain Energy

A RC beam element that has been strengthened is also subjected to a net axial compressive force of magnitude F_p (F_p=force in the FRP plate) at the centroid (Fig. 2). The axial strain energy in the segment of unit length ($\text{SE}_E|_{\text{axial}}$) can be calculated as

$$\text{SE}_E\big|_{\text{axial}} = \frac{1}{2}F_p\varepsilon_0 \tag{2}$$

ε_0=centroidal strain, calculated from

$$\varepsilon_0 = \kappa_L \times (x_L - \alpha) \tag{3}$$

where α=section's centroidal axis depth; and x_L=neutral axis depth of the section.

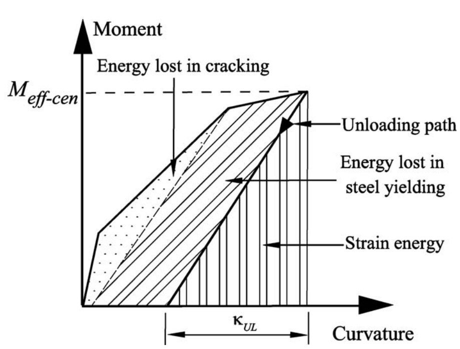

Fig. 3. Energy in flexure

This assumes that the reinforced section behaves linearly elastically for axial force up to the loading in question, which is not exactly correct, but is a reasonable approximation, and it is found in practice that this component of the strain energy is rarely more than about 5% of the total. A more complex analysis, which would follow the load-extension response, and allow for continuing variations in the position of the neutral and centroidal axes, is not justified.

Full details of the present-extent-of-cracking concept (C_x) can be found in Achintha and Burgoyne (2006), but are summarized here.

The neutral axis position x_L can be directly found from the section analysis for an uncracked or a fully cracked section ($x_L|_{\text{uc}}$ and $x_L|_{\text{fc}}$, respectively), and by interpolation for a partially cracked section. Thus, x_L of a partially cracked section becomes

$$x_L = C_x\, x_L\big|_{\text{uc}} + (1 - C_x)\, x_L\big|_{\text{fc}} \tag{4}$$

The interpolation coefficient C_x represents the extent of cracking of the section and is given by

$$C_x = \left(\frac{M_{\text{cr-mid}}}{M_{\text{app-mid}}}\right)^{3.5}\left[1 - \left(\frac{M_{\text{app-mid}} - M_{\text{cr-mid}}}{M_{\text{y-mid}} - M_{\text{cr-mid}}}\right)^{3.5}\right] \tag{5}$$

where $M_{\text{cr-mid}}$, $M_{y\text{-mid}}$, and $M_{\text{app-mid}}$=moments effective on the RC section about its middepth axis at the externally applied moments M_{cr}, M_y, and the given M_{app} ($M_{\text{cr}} < M_{\text{app}} < M_y$). The model is based on Branson's concept (Branson 1968), but slightly modified so that first cracking and the first yielding of the tension steel define the uncracked and fully cracked states. Only that part of the effective moment that acts on the RC section is used to represent the extent of cracking, and account is also taken of the axial force induced in the RC section. To avoid unrealistic contributions due to varying eccentricities of the force in the FRP, a fixed reference axis will be used for the comparison; the middepth axis of the beam is chosen. The centroidal and neutral axes, which are not coincident, are both interpolated following the work of Sakai and Kakuta (1980).

Strain Energy in the FRP Plate

The FRP plate is assumed to be linear elastic so the strain energy in a unit length is

$$\text{SE}_E\big|_{\text{FRP}} = \frac{1}{2}\frac{F_p^2}{E_pA_p} \tag{6}$$

where E_p and A_p=elastic modulus and the cross-sectional area of the FRP plate, respectively.

Once the energy state of the strengthened beam under the given loading state is known, energy conservation concepts can be used to determine the energy released from the system when the existing debonding crack extends.

Energy Available for Debonding

It is necessary to calculate the energy state before and after propagation of the debonding crack. It is assumed that the applied load (P) remains constant during the fracture increment, but the structure loses stiffness because of the removal of the compatibility condition where the new crack forms. Thus, the overall deflection will become larger, increasing the work done by the external load and adding to the system's strain energy [Fig. 4(a)]; there will also be a redistribution of the way the energy is stored within the beam. The FRP plate is assumed to be linear elastic so energy

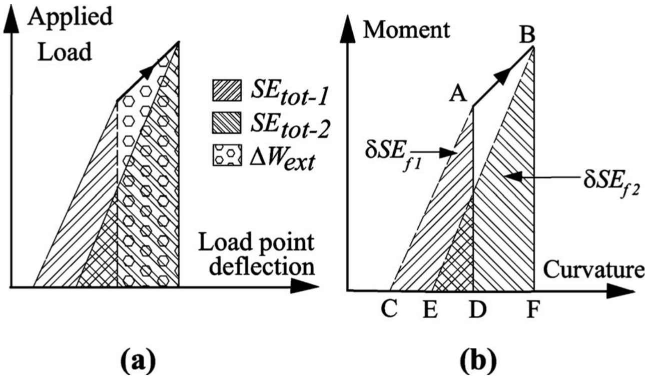

Fig. 4. Energy balance (a) load-deflection plot (complete system); (b) $M-\kappa$ plot (RC segment)

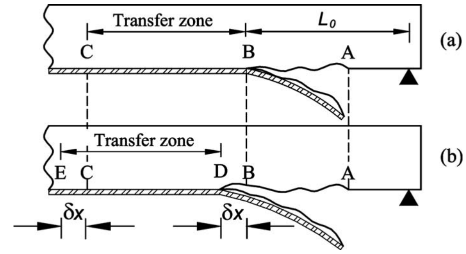

Fig. 5. Energy release zones for plate-end debonding

losses only occur within the RC section due to changes in the flexural and axial actions, which can be determined by knowledge of the moment-curvature and axial force-centroidal strain relations.

Thus, the energy balance can be represented by

$$\Delta W_{\text{ext}} = (\text{SE}_{\text{tot}-2} - \text{SE}_{\text{tot}-1}) + \Delta E_{\text{loss-tot}} \tag{7}$$

where ΔW_{ext}=change in the external work done on the system; and $\text{SE}_{\text{tot}-1}$ and $\text{SE}_{\text{tot}-2}$=total strain energy of the system before and after the debonding crack extension; and $\Delta E_{\text{loss-tot}}$=energy lost during the process.

That loss is made up of three portions

$$\Delta E_{\text{loss-tot}} = \Delta E_{\text{loss}-f} + \Delta E_{\text{loss}-a} + \Delta \text{ER}_d \tag{8}$$

where $\Delta E_{\text{loss}-f}$ and $\Delta E_{\text{loss}-a}$=energy losses due to change in flexural actions and the axial actions on the RC sections, respectively. The final term (ΔER_d)=energy available for debonding, and its magnitude, when compared with the energy needed to form the fracture, is the key factor in deciding whether the crack will propagate.

Energy Loss due to Change in Flexural Actions

If the moment applied to the RC element alone ($M_{\text{eff-cen}}$) increases with the debonding crack extension, some of the additional external work done is associated with this transformation. Part of this causes an increase in the flexural strain energy and the rest is lost due to material nonlinearity. Points A and B in the M-κ plot given in Fig. 4(b) represent a section of unit length before and after the debonding-crack extension; areas ACD (δSE_{f1}) and BEF (δSE_{f2}) represent the respective flexural strain energies. The associated external work done (δW_f) is represented by area ABFD of Fig. 4(b). The energy lost $\delta E_{\text{loss}-f}$ can be found from the energy conservation

$$\delta W_f = (\delta \text{SE}_{f2} - \delta \text{SE}_{f1}) + \delta E_{1\text{oss}-f} \tag{9}$$

If $M_{\text{eff-cen}}$ reduces with the debonding crack extension, no energy lost takes place because the materials are assumed to unload elastically (Achintha and Burgoyne 2006).

The total energy loss in the complete beam ($\Delta E_{\text{loss}-f}$) due to change in flexural actions can be found by integrating the $\delta E_{\text{loss}-f}$ at each cross section.

Energy Loss due to Change in the Net Axial Force

In a similar way, the energy loss due to change in the net axial force on the RC portion ($\Delta E_{\text{loss}-a}$) must also be determined according to the relative magnitudes of F_p before and after the crack extension, with the centroidal strain determined from Eq. (3).

It is now possible to determine the total energy release from the system upon debonding-crack extension, but first, the zones of the beam from which energy can be released have to be identified.

Energy Release Zones for Plate-End Debonding

When an FRP plate is curtailed at a nonzero moment location, the axial strain difference between the plate end and the concrete immediately adjacent to it (i.e., zero axial strain in the FRP and a nonzero strain in the concrete) causes relative slip between the two adherents in the vicinity of the plate end. Thus, for a section near the plate end, the relevant F_p cannot be determined by assuming a unique linear strain distribution across both the beam and the plate, despite the plate still being "bonded" to the beam. This slip and the corresponding shear stresses are assumed to decay in an exponential manner, and are significant only over a transfer zone (Täljsten 1997). For a section outside the transfer zone, a linear strain distribution across both the FRP plate and the beam can be assumed because the plate is here fully bonded.

The externally applied loads on the beam are assumed to remain unchanged during crack extension, so for a fully bonded section, F_p and the strain profiles, and hence the energy state, cannot be altered due to the crack extension. Thus, no energy is released from the fully bonded sections. However, the F_p profile changes over the transfer zone due to the crack extension, and energy releases are expected as described above.

Identification of the Energy Release Zones

Fig. 5(a) shows a strengthened beam with an assumed plate-end debonding crack AB, and the region BC=relevant transfer zone. The crack then extends by a small distance δx [Fig. 5(b)]. Assuming that the transfer zone length is fixed for the given system, the zone DE=new transfer zone. The plate carries no force over the zone AB during both stages and, hence, neither the strain profiles nor the energy states of the relevant sections are altered by the transformation, and there is no associated energy release. Similarly, there are no energy releases from the sections to the right of E [Fig. 5(b)] as those are fully bonded. The narrow zone BD was initially within the transfer zone, and, thus, carried some force in the FRP, but after the crack extension, the FRP is ineffective. The zone CD is within the transfer zone for both stages, but the F_p profiles have changed. The narrow zone CE has changed from the fully bonded state to the transfer state. In all three regions, the stress distribution has changed so some energy will have been released.

The strain energy calculations of the sections with known F_p values are performed as described above, but for the sections with no effective FRP (sections within zone AB before extension and AD afterwards), only the flexural energy must be considered. However, the F_p profile within the transfer zone, and the length of the transfer zone (L_t), are both required for the total energy release determination.

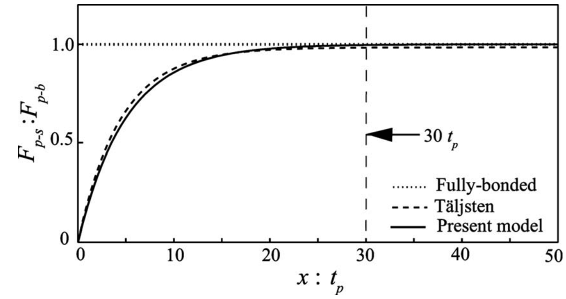

Fig. 6. Transfer zone F_p profile

FRP Force Distribution in the Transfer Zone

A detailed analysis of the transfer zone, taking account of all the material nonlinearities and the tension-stiffening effects of cracked concrete is virtually impossible to perform. Linear-elastic solutions have been presented, for example that by Täljsten (1997), which reveal that the effects of the plate-end slip decay exponentially.

Within the transfer zone, the stress transfer between the RC beam and the FRP plate primarily depends on the stiffness of the plate and the interface shear-stress/relative-slip characteristics. Neither the nonlinear behavior of the concrete nor the presence of cracks in the RC beam have significant effects on the interface stress transfer. It is believed that Täljsten's analysis (Täljsten 1997) adequately represents the stress transfer between the FRP plate and the beam, irrespective of the amount of nonlinearity.

Proposed Expression for Transfer Zone FRP Force Profile

Täljsten's analysis, which was designed to determine the stress distribution in the vicinity of the plate end, predicts that the interface shear stresses decay exponentially; the force in the FRP plate ($F_{p-s}|_{x=x}$) is, therefore, assumed to vary as

$$F_{p-s}\big|_{x=x} = F_{p-b}\big|_{x=x} - F_{p-b}\big|_{x=0} \times e^{-\lambda x} \tag{10}$$

where $F_{p-b}|_{x=x}$=force that would exist in the FRP at a position x from the plate end (but within the transfer zone) if it was fully bonded to the concrete. Täljsten's expression for the length scale λ involved the properties of the FRP plate, the concrete, and the adhesive, but for most practical beams, only the variations in the FRP and the adhesive properties make a significant difference, so it is proposed here that λ be taken as

$$\lambda = \sqrt{\frac{G_a}{t_a} \times \frac{1}{E_p t_p}} \tag{11}$$

where G_a and t_a=shear modules and the thickness of the adhesive; and E_p and t_p=Young's modulus and the thickness of the FRP plate, respectively. Comparisons between the predictions based on Eq. (10) and the original Täljsten (1997) expressions have been made for a large number of beam specimens covering many variations of geometric, loading, and material properties. A typical result is shown in Fig. 6; the force in the FRP has been nondimensionalized with respect to the force expected if the FRP was perfectly bonded to the concrete. Täljsten's result remote from the end differs very slightly from this because he allows for the elasticity in the adhesive, which is ignored here. The curves are otherwise close enough for all practical purposes and show that a transfer zone length of 30 times the FRP plate thickness is sufficient. This value is used in all subsequent analyses.

Energy Release Zones for Midspan Debonding

The midspan debonding analysis is more complicated than that of the plate-end debonding, because there exist two end regions, both fully bonded, separated by a region in which the FRP plate is debonded but still constrained by a compatibility condition (Fig. 7).

At each boundary of the debonded zone, the unbonded F_p gradually reaches the fully bonded value. Thus, when the crack extends, the resultant variations in F_p over both the debonded zone and the transition zones should be considered in the determination of the total energy release. The values of F_p in the bonded zone at the boundary and in the debonded region can be determined in a separate analysis, and the transition between them is assumed to vary exponentially using the same characteristic length λ described above. The change in force at the boundary between the two regions can be positive or negative, depending on the circumstances.

The unbonded F_p is determined by equating the *extension* of the FRP plate in the debonded region with the extension of the tension fiber in the concrete over the same zone. Account is also taken of the relative slip between the FRP and the RC beam in the transition zones [as discussed in the derivation of Eq. (10)], but the effect is normally marginal.

Energy Release Rate

It is now possible to determine the energy release rate (G_R), the energy release per unit area of crack extension, when the existing debonding crack propagates. The zones where energy is being dissipated (the transfer zone for plate-end debonding, the debonded zone, and the two transition zones for midspan debonding) are divided into short segments and the energy computations are performed for each segment before and after the assumed debonding-crack extension. The energy terms in Eqs. (7) and (8) are obtained by summing the individual terms in all segments, and the deflection profiles required to determine the external work done are computed by the numerical integration of the curvatures. The total energy release at the debonding-crack tip ($\Delta \mathrm{ER}_d$) is obtained from Eq. (8). The energy release rate (G_R) is

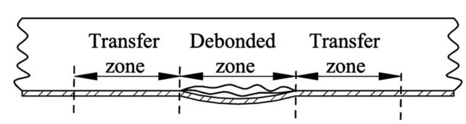

Fig. 7. Energy release zones for midspan debonding

$$G_R = \frac{\Delta \mathrm{ER}_d}{b_p \delta x} \quad (12)$$

where b_p and δx=width of the FRP plate and the horizontal-linear crack extension, respectively.

G_R can then be compared with the energy required to fracture a unit area of the interface, (G_F) to decide whether the crack will extend or not. If $G_R \geq G_F$, the crack will extend causing debonding; if not, there is insufficient energy for the crack to propagate.

Due to the material heterogeneities and the complex loading conditions present at the tip, crack extension will not take place on a unique plane so G_R in Eq. (12) represents the energy release per unit area of crack projected onto the horizontal plane. Nevertheless, G_R calculated this way can still be compared with the interface fracture energy (G_F), which is either experimentally determined or based on an existing theoretical model, both of which include accounts for inevitable tortuous fracture propagations.

Concrete-FRP Interface Fracture Energy

It is now necessary to determine the concrete-FRP interface fracture energy (G_F). The propagation of an interface crack takes the path requiring least energy. Experimental evidence confirms that concrete-FRP debonding fractures generally propagate through the concrete just above the interface (Leung 2001; Buyukozturk et al. 2004). It is, however, reported that due to poor surface preparation prior to plate bonding or the use of low-strength adhesives, the debonding fractures can propagate along the interface or within the adhesive (Buyukozturk et al. 2004). With the availability of high-strength adhesives and careful surface preparation techniques, these adhesive and interface failures can be precluded. Thus, the present work concentrates only on the case where the debonding fractures propagate through the concrete, as this is the actual problem encountered in the industry.

Fracture Mode of the Interface Concrete

Since the debonding fractures propagate through the concrete, the interface fracture energy (G_F) is that of the concrete. In the vicinity of the interface, both normal and shear stresses are inevitable, so it would be expected that debonding fractures are governed by mixed-mode effects. The fracture energy and the fracture trajectories of concrete under mixed-mode loading have been the subject of many experiments (Bocca et al. 1991; Gálvez et al. 2002). The relevant numerical simulations were mostly performed by incorporating the cohesive crack model (Hillerborg et al. 1976) and the maximum principal tensile stress criterion (Erdogan and Sih 1963) into finite-element codes, and confirmed that, even under mixed-mode conditions, concrete fractures grow locally in a pure Mode I state (Bocca et al. 1991; Gálvez et al. 2002). The present study is concerned with the start of the fracture process, so Mode II effects, such as aggregate interlock, are not relevant.

Mode I Fracture Energy of Concrete

In concrete, the nonlinear fracture process zone (FPZ) ahead of a preexisting crack tip is relatively large compared to the structural dimensions, and, therefore, its effects should not be neglected as is done in linear elastic fracture mechanics. Material softening taking place in the FPZ should be taken into account in the estimation of Mode I fracture energy of concrete (G_{IC}). Hillerborg's fictitious crack model (Hillerborg et al. 1976), which represents G_{IC} as the area under the corresponding softening-stress/crack-surface-separation ($\sigma - w$) curve, is widely believed to be the best available simple nonlinear concrete fracture model (Bažant et al. 2002). The exact σ-w relations of a given concrete can only be known from direct uniaxial tensile tests, but models that describe the softening curve in terms of more readily available parameters of the concrete, based on databases of test results, have been proposed in the literature (Gustafsson and Hillerborg 1984; Reinhardt 1985; Guinea et al. 1994). The corresponding values for G_{IC} for the concrete assumed in the example described in the later part of this paper [compressive strength, $f'_c = 35\ \mathrm{N/mm^2}$, tensile strength, $f_t = 3.7\ \mathrm{N/mm^2}$, maximum aggregate size, $d_{\max}$ (crushed)=20 mm, and water cement ratio, $w/c = 0.5$], together with the estimations based on two reported empirical models of G_{Ic} [CEB-FIP model code (1991) and Bažant and Becq-Giraudon (Bažant et al. 2002)] are given in Table 1.

Table 1. G_{IC} Estimation

Reference	Model type	G_{IC} (N/mm)
Gustafsson and Hillerborg (1984)	Bilinear softening	0.154
Reinhardt (1985)	Power relation	0.093–0.159
Guinea et al. (1994)	Bilinear softening	0.162
CEB-FIP model code (1991)	Empirical	0.0825 ± 0.025
Bažant et al. (2002)	Empirical	0.112 ± 0.034

Some of the above $\sigma - w$ models require knowledge of the critical crack opening displacement of the concrete (i.e., the lowest crack opening that gives zero tensile stress w_c), but this is not usually available, so predictions are based on the $w_c$values reported by Hilsdorf and Brameshuber (1991).

Guinea et al. (1994) predicted the softening curve from measured values of G_{IC} to determine the critical parameters. The way in which G_{IC} depends on these parameters has been taken from the CEB-FIP model code and the Bažant and Becq-Giraudon empirical expressions, and these have been used to extrapolate the predictions of Guinea's model for the particular concrete used here.

The Reinhardt (1985) model gives a range of values (quoted in Table 1) to be expected from tests but does not give a method for predicting the exact value without doing a test.

The empirical G_{IC} expression given in the CEB-FIP model code (1991) is the simplest to use because it is based on the strength of concrete and the maximum aggregate size, but it is based on a relatively small database, determined according to the RILEM Committee 50-FMC (1985) standards (Hilsdorf and Brameshuber 1991). It is believed that this test underestimates G_{IC}, because it assumes that full strain softening occurs at the existing notch tip, which is unrealistic in most laboratory-scale test specimens (Guinea et al. 1994; Bažant et al. 2002). Thus, the CEB-FIB expression underestimates G_{IC}. Bažant and Becq-Giraudon's empirical expression (Bažant et al. 2002) accounts for the full softening and is based on a much larger database, taking account of more parameters, some of which have significant effects on G_{IC} of concrete, such as, for example water cement ratio and type of aggregate.

The two bilinear models predict similar G_{IC} and also agree with Reinhardt's power relation model and the Bažant and Becq-Giraudon empirical expression predictions (Table 1). The CEB-FIB model code expression gives a lower value, but is thought to be less reliable because it uses a smaller sample. In the debonding analysis presented below, a value of $0.15\ \mathrm{N\,mm/mm^2}$ (N/mm) is taken for G_{IC}.

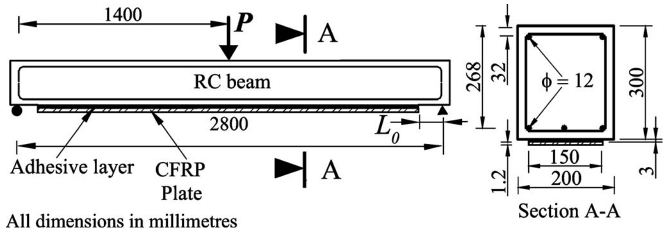

Fig. 8. Specimen dimension and loading data

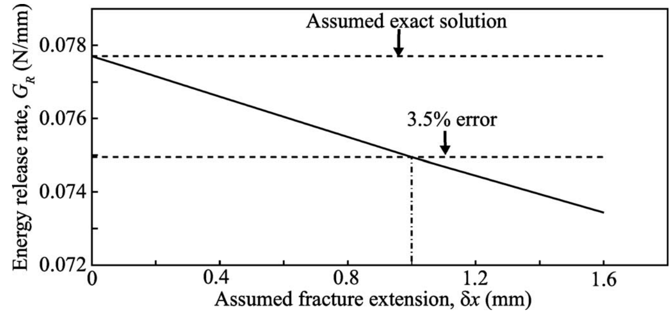

Fig. 10. Size independency of G_R

A later RILEM report RILEM Committee 89-FMT (1991) includes improved proposals for the experimental evaluation of G_{IC}. Notched-beam specimens are recommended for the experimental programs; in conjunction with the correct size-effect laws, these experiments can estimate the size-independent G_{IC} of a given mix. The experimentally evaluated size-independent G_{IC} of mixes with similar properties to the current mix agree well with the assumed value of 0.15 N/mm (Karihaloo et al. 2003).

Example

To illustrate the application of the model, a RC beam, strengthened with a carbon fiber reinforced polymer (CFRP) plate, and loaded as shown in Fig. 8, has been analyzed. Details of the assumed material behavior are given elsewhere (Achintha and Burgoyne 2006); only the numerical values are presented here. The compressive and the tensile strengths of the concrete are assumed to be 35 and 3.7 N/mm^2 and the Young's modulus and the yield stress of steel are taken as 200 kN/mm^2 and 530 N/mm^2, respectively. The shear modulus of the adhesive is taken as 2 kN/mm^2 and the Young's modulus of the CFRP is 165 kN/mm^2. The unstrengthened capacity of the beam is 65 kN; after strengthening with CFRP, the failure load should be about 145 kN, assuming that debonding does not take place. The failure mode would have changed from an underreinforced failure before strengthening to an overreinforced mode afterwards.

Plate-End Debonding

Fig. 9(a) shows the variation in energy release rate (G_R) if debonding occurs at different load levels, for different locations of the plate curtailment position L_0 (measured from the support). Increasing either the applied load (P) or L_0 means that the transfer zone sections are subjected to higher applied moments and are, thus, less stiff, either because of concrete cracking and/or yielding of the steel. This means that there is more energy available for release so G_R increases.

The same figure also shows that if L_0 is less than about 335 mm, the energy release rate is less than G_{IC} and no plate-end debonding would occur before the beam reached its flexural capacity (145 kN). If L_0 is greater than 335 mm, it is predicted that premature debonding failure would occur at lower loads. Fig. 9(b) shows the failure load against L_0 and shows how far the plate should extend so that additional external anchoring devices are not needed.

It is worth noting that, since the peeled plate can effectively be ignored since it carries no force, the case of a longer plate with a debonding flaw can be modeled by measuring L_0 from the tip of the crack rather than the end of the plate.

Convergence of the Results

One of the main drawbacks associated with the finite-element analyses for plate debonding problems is the dependency on the size of the element used. The models tend to predict infinite stress concentrations at the plate ends when small elements are used. It is, therefore, important to investigate the effect of the step size (i.e., the assumed fracture extension, δx) in the present analysis. Fig. 10 shows the calculated energy release rate (G_R) against the step size (δx) selected for the case of L_0=300 mm when P is 140 kN. This shows that the results are virtually independent of the selected δx and gives an error of about 3.5% when δx is 1 mm, which is well within the accuracy within which G_{IC} is known. Smaller values of δx can be used, but they can give rise to numerical convergence problems. All the other analyses presented here are based on δx of 1 mm.

In the numerical computation, the transfer zone is divided into

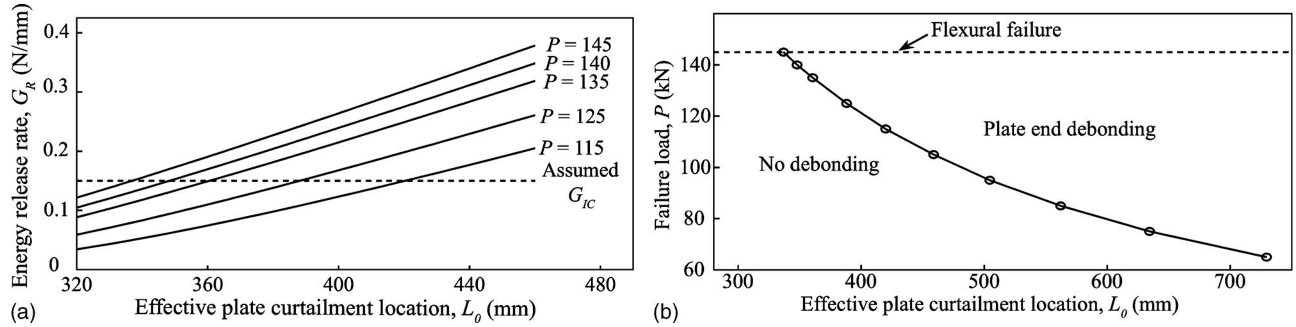

Fig. 9. Plate-end debonding (a) G_R for different L_0 and P; (b) failure load against L_0

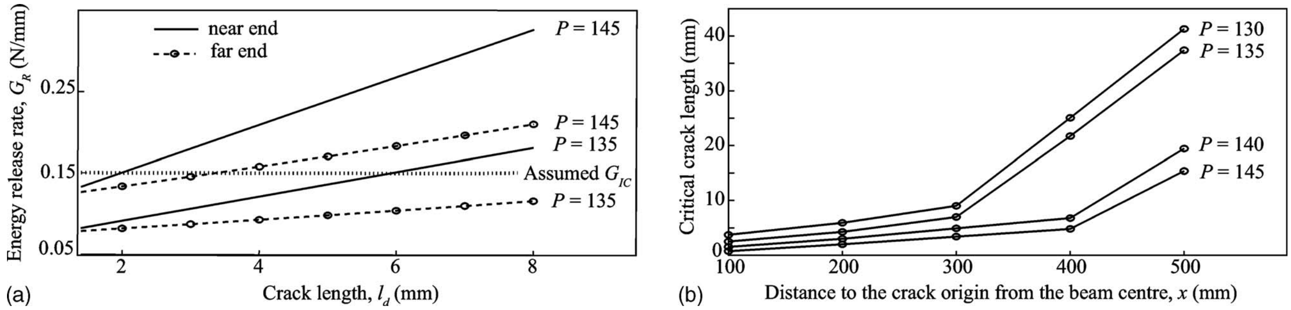

Fig. 11. Midspan debonding (a) G_R for different l_d at a fixed crack origin; (b) critical l_d for different crack locations at different P

narrow segments within which the moment is assumed to be constant. After crack extension, the distance to the center of a given segment from the effective plate end (x) changes, thus, causing a change in the F_p effective in that segment. Segment sizes have been chosen to be of the same order of magnitude as δx. Studies of the detailed results show that most of the energy release takes place in the portion of the transfer zone closest to the unbonded region (<5 times the plate thickness t_p). The number of segments to analyze and, hence, the computational time can be reduced by selecting relatively thicker segments (e.g., segments of lengths of the same order of magnitude as t_p) at the other end of the transfer zone.

Midspan Debonding

Fig. 11(a) shows G_R for a fracture propagating from an internal crack, one end of which is 200 mm from the centerline, with a crack length of l_d. This shows that if l_d exceeds about 2 mm, debonding would occur towards the nearest end support at a load less than the strengthened capacity of the beam (145 kN). Debonded lengths of this sort of dimension may well be present, and undetectable, in many practical applications. If the initial fracture is longer than this, debonding will take place at lower loads.

The possibility that the fracture might extend in the opposite direction has also been studied [as shown in Fig. 11(a) by dashed lines], but these show that more load, or a higher crack length, would be required to propagate in this direction, so it is unlikely to be critical.

Fig. 11(b) shows contour plots of the load at which midspan debonding will take place against the debonding crack length and its location. Short cracks that start near midspan (on the left of the diagram), where the section is cracked in flexure at both the debonded zone and in the transfer zone, propagate more easily, and start at lower loads. In contrast, if the crack starts further away from the centerline (to the right of the diagram), the bending moments are lower; there is less flexural cracking and there is less strain energy that can be released. The effect is that more load, or a longer crack, is needed to cause debonding. The sudden change in the critical crack length, shown in Fig. 11(b) occurs when the debonded zone and the transition zone change from being uncracked to being partially cracked (on the right of the diagram), and later fully cracked (on the left).

Studies of the detailed results show that, for shorter crack lengths, most of the strain energy changes occur in the transfer zones, because these are relatively long. However, on one side of the crack, the strain energy increases, while on the other it decreases. The results also show that, although the axial strain energy stored in the concrete is quite small, the contribution to the release rate can be as high. These aspects are the objects of further investigation.

Conclusions

The study has shown that the phenomena of plate debonding can be studied by means of a fracture-mechanics energy-release-rate approach, which obviates the need for a finite-element analysis of dubious validity.

It has been necessary to produce a modified form of Branson's method to allow the calculation of the strain energy of a section when it is partially cracked and when subjected to an axial load imposed by the FRP plate.

Hutchinson's interface fracture model has proved to be a very useful tool for the study of the debonding of FRP plates from concrete structures. More work remains to be done to study the importance of the various parameters that influence the result. Comparisons with experimental data in the literature are being undertaken, as is a parametric study.

Acknowledgments

The first writer was sponsored in this work by the Overseas Research Studentships (ORS) and the Cambridge Commonwealth Trust, and is appreciative of their financial assistance.

References

Achintha, P. M. M., and Burgoyne, C. J. (2006). "Moment-curvature and strain energy of beams with external FRP reinforcement." *ACI Struct. J.*, preprint available at ⟨http://www-civ.eng.cam.ac.uk/cjb/frpdebond/⟩.

American Concrete Institute (ACI). (2002). "Guide for design and construction of externally bonded FRP systems for strengthening concrete structures." *ACI 440.2R-02*, ACI Committee 440, Farmington Hills, Mich.

Bažant, Z. P., Yu, Q., and Zi, G. (2002). "Choice of standard fracture test for concrete and its statistical evaluation." *Int. J. Fract.*, 118(4), 303–337.

Bocca, A., Carpinteri, A., and Valente, S. (1991). "Mixed mode fracture of concrete." *Int. J. Solids Struct.*, 27(9), 1139–1153.

Branson, D. E. (1968). "Design procedures for computing deflections." *ACI J.*, 65(9), 730–735.

Buyukozturk, O., Günes, O., and Karaca, E. (2004). "Progress on understanding debonding problems in reinforced concrete and steel members strengthened using FRP composites." *Constr. Build. Mater.*, 18(1), 9–19.

Chen, X. (2006). "Calcium-magnesium-alumina-silicate (CMAS) delamination mechanisms in EB-PVD thermal barrier coatings." *Surf. Coat. Technol.*, 200(11), 3418–3427.

Comite Euro-International du Beton-Federation Internationale de la Precontrainte (CEB-FIP) model code. (1991). Lausanne, Switzerland.

Daily, J. S., and Klingbeil, N. W. (2006). "Plastic dissipation in mixed-mode fatigue crack growth along plastically mismatched interfaces." *Int. J. Fatigue*, 28(12), 1725–1738.

Erdogan, F., and Sih, G. C. (1963). "On the crack extension in plates under plane loading and transverse shear." *J. Basic Eng.*, 85, 519–527.

Gálvez, J. C., Cendón, D. A., and Planas, J. (2002). "Influences of shear parameters on mixed-mode fracture of concrete." *Int. J. Fract.*, 118(2), 163–189.

Guinea, G. V., Planas, J., and Elices, M. (1994). "A general bilinear fit for the softening curve of concrete." *Mater. Struct.*, 27(2), 99–105.

Günes, O. (2004). "A fracture based approach to understanding debonding in FRP bonded structural members." Ph.D. thesis, Massachusetts Institute of Technology, Cambridge, Mass.

Gustafsson, P. J., and Hillerborg, A. (1984). "Improvements in concrete design achieved through the application of fracture mechanics." *Application of fracture mechanics to cementitious composites*, NATO Advanced Research Workshop, Evanston, 639–680.

Hearing, B. P. (2000). "Delamination in reinforced concrete beams retrofitted with fibre reinforced plastics." Ph.D. thesis, Massachusetts Institute of Technology, Cambridge, Mass.

Hillerborg, A., Modéer, M., and Peterson, P. E. (1976). "Analysis of crack formation and growth in concrete by means of fracture mechanics and finite elements." *Cem. Concr. Res.*, 6(6), 773–782.

Hilsdorf, H. K., and Brameshuber, W. (1991). "Code-type formulation of fracture mechanics concepts for concrete." *Int. J. Fract.*, 51(1), 61–72.

Hutchinson, J. W., and Suo, Z. (1992). "Mixed mode cracking in layered materials." *Adv. Appl. Mech.*, 29, 63–191.

Karihaloo, B. L., Abdalla, H. M., and Imjai, T. (2003). "A simple method for determining the true specific fracture energy of concrete." *Mag. Concrete Res.*, 55(5), 471–481.

Kay, N. R., Ghosh, S., Guven, I., and Madenci, E. (2006). "A combined experimental and analytical approach for interface fracture parameters of dissimilar materials in electronic packages." *Mater. Sci. Eng., A*, 421(1–2), 57–67.

Leung, C. K. Y. (2001). "Delamination failure in concrete beams retrofitted with a bonded plate." *J. Mater. Civ. Eng.*, 13(2), 106–113.

Liu, X. H., Lane, M. W., Shaw, T. M., and Simonyi, E. (2007). "Delamination in patterned films." *Int. J. Solids Struct.*, 44(6), 1706–1718.

Pham, H. B., and Al-Mahaidi, R. (2006). "Prediction models for debonding failure loads of carbon fibre reinforced polymer retrofitted reinforced concrete beams." *J. Compos. Constr.*, 10(1), 48–59.

Reinhardt, H. W. (1985). "Crack softening zone in plain concrete under static loading." *Cem. Concr. Res.*, 15(1), 42–52.

RILEM Committee 50-FMC. (1985). "Determination of the fracture energy of mortar and concrete by means of the three-point bend tests on notched beams." *Mater. Struct.*, 18(4), 287–290.

RILEM Committee 89-FMT. (1991). *Fracture mechanics test methods for concrete*, 1st Ed., Cambridge Univ. Press, Cambridge, U.K.

Sakai, K., and Kakuta, Y. (1980). "Moment-curvature relationships of reinforced concrete members subjected to combined bending and axial force." *ACI J.*, 77(3), 189–194.

Täljsten, B. (1997). "Strengthening of beams by plate bonding." *J. Mater. Civ. Eng.*, 9(4), 206–212.

Vellinga, W. P., Timmerman, R., van Tijum, R., and De Hosson, J. T. M. (2006). "Microscopic aspects of crack propagation along PET-glass and PET-Al interfaces." *Int. J. Solids Struct.*, 43(24), 7371–7377.